## PAPER

Check for updates

# Nitrogen regulation in polyester-based carbons and adsorption of gaseous benzene and ethyl acetate†

Gang Wang,[a] Pingping Tan,[a] Ziyan Kong,[a] Jianfang Ao,[b] Ran Wang,*[a] Zhongshen Zhang[c] and Zhengping Hao [ID] *[c]

Nitrogen doping effectively improves the adsorption properties of activated carbons towards volatile organic compounds (VOCs); however, the role of nitrogen elements with various chemical valence states need further evaluation. In this work, waste polyester fabrics were used as a low-cost source to prepare activated carbon, and melamine, pyridine, dimethylamine, and pyrrole were selected as nitrogen sources to compare their nitrogen-doping ability. The adsorption of low-concentration benzene and ethyl acetate on the resultant carbons and the effects of nitrogen, including its valence states and contents, were investigated. Characterizations showed that the nitrogen contents of carbons after doping with melamine (C-M), pyridine (C-P), dimethylamine (C-D), and pyrrole (C-Y) increased, while their corresponding specific surface areas were about 32.6%, 72.2%, 142% and 14.3%, respectively, of the original carbon value of 188.7 $cm^2$ $g^{-1}$. Dynamic breakthrough experiments verified the increase in adsorbed amounts of both non-polar benzene and polar ethyl acetate molecules, with a more significant enhancing effect on benzene. The specific surface area and pore volume mainly contribute to the adsorbed amounts. Regarding the influence of nitrogen-containing functional groups, pyridinic nitrogen was more conducive to benzene adsorption under dry conditions because of the stronger $\pi-\pi$ interaction and N−H hydrogen bond; however, its water resistance was inferior to that of pyrrolic nitrogen. Saturated C-P can be effectively regenerated and the adsorbed capacity of benzene remained about 75% after five adsorption cycles. The increased adsorbed amount and super regeneration property identify pyridine as a nitrogen source with priority consideration in the nitrogen modification of activated carbons for VOC adsorption.

## 1. Introduction

Volatile organic compounds (VOCs) are widely used in paints, adhesives, and chemical detergents for their unique characteristics such as low boiling point, high vapor pressure, and good compatibility with organic substances.[1,2] However, inevitable volatilization and leakage from industrial point sources pose severe threats to the ecological environment. VOCs act as an important precursor of ozone and fine particulate matter ($PM_{2.5}$), accelerate photochemical reactions, and finally cause complex regional atmospheric pollution.[3–5] Besides, they are harmful to humans: exposure to VOCs leads to a range of

[a]*School of Material Design & Engineering, Beijing Institute of Fashion Technology, Beijing, 100092, China. E-mail: clywr@bift.edu.cn*

[b]*Hubei Weipu Testing Technology Co., Ltd, Wuhan, 430205, China*

[c]*National Engineering Laboratory for VOCs Pollution Control Material & Technology, Research Center for Environmental Material and Pollution Control Technology, University of Chinese Academy of Sciences, Beijing, 101408, China. E-mail: zphao@ucas.ac.cn*

† Electronic supplementary information (ESI) available. See DOI: https://doi.org/10.1039/d4ra07004f

adverse health effects such as nausea, mucosal irritation, and even cancer.[6,7] Thus, the elimination of VOCs is particularly necessary, and a series of technologies have been developed.[8]

Based on whether the structure of VOC molecules is destroyed, all technologies used for the control of VOCs can be divided into two categories, *i.e.*, recovery and destruction methods.[1] For example, incineration, bio-degradation, and advanced oxidation are destruction methods, while absorption, adsorption, and condensation belong to the recovery method.[9,10] At the current stage, adsorption is widely used because of its high efficiency, simple operation process, and low energy consumption. The adsorbent plays the most critical role in the whole adsorption system, and zeolite, silica gel, and activated carbon constitute the commonly used adsorbents.[11] Among them, its developed pore structure and adjustable surface chemistry make activated carbon the most suitable candidate in the regime of adsorption.[12]

In view of their porous structure, activated carbons are solid and amorphous; composed of lamellar graphite, which is stacked layer by layer and form a large number of mesoscopic and microscopic inner pores.[13] At the edge of the stacked

graphite layer, various functional groups are suspended, of which the nitrogen-containing groups are considered to be propitious for the adsorption of VOCs.[14–16] For example, Shi et al. found that the total nitrogen content was positively correlated with the toluene adsorption capacity.[17] Li et al. verified that the introduction of nitrogen atoms using ammonia solution increased the adsorption capacity of hydrophobic o-xylene on activated carbon by 26.5%.[18] Zhang et al. added urea as a nitrogen source during the carbonization process of MIL-101, and the adsorbed amount of benzene on the resultant N-doped carbon was about two times that on the undoped carbon.[19] The underlying mechanism of how these nitrogen-containing functional groups affect adsorption has always been a focus of research. Actually, the nitrogen element in the nitrogen-containing functional groups exhibits different valence states, and their contributions to the adsorption properties of carbons are different. For example, Zhu et al. found it was pyrrolic/graphitic nitrogen that enhanced the hydrophobicity of carbons; thus, the adsorbed amounts of p-xylene increased under the condition of high humidity.[20] Li et al. believed the promotion of hydrophobicity mainly came from graphitic nitrogen and pyridinic nitrogen which reinforced the π–π interactions between carbon and toluene molecules.[21] However, some studies presented the opposite phenomena. Fan et al. found that pyridinic and pyrrolic nitrogen could enhance the adsorption of water by increasing the electrostatic interaction between water molecules and carbon, thus inhibiting the adsorption of benzene.[22] Jiao et al. and Zhao et al. found that pyrrolic nitrogen and graphitic nitrogen in some cases were beneficial to the adsorption of polar VOCs, such as methanol and formaldehyde.[23,24] These inconsistent results reflect the complexity of nitrogen-functional groups in affecting the adsorption performances of activated carbons. One possible reason may be that the effects of nitrogen with different valence states and the structural parameters of the adsorbent are intertwined during the adsorption process; thus, accurately distinguishing the contribution of each part is quite difficult.[25]

Activated carbons are usually prepared through carbonization and activation of both chemical and biological raw materials.[18,26] As a typical alternative, waste polyester fibers have received great attention in recent years.[27–29] Xu et al. prepared activated carbon using polyester fabric wastes with different iron salts as activators. The adsorbed amount of Black T, a typical azo dye, on the carbon activated by chlorinated iron reached 450.23 mg g$^{-1}$, showing a better activation effect of iron dichloride than ferrous sulfate.[30] Duman et al. used zinc chloride and potassium hydroxide to activate polyester wastes and compared their adsorption properties towards oxytetracycline from aqueous solutions. The adsorbed amount on carbon activated by zinc chloride was about 1.5 times that of potassium hydroxide.[31] Serras-Malillos et al. optimized the pyrolysis conditions of reinforced polyester and obtained three products, including coke, very little aqueous liquid and synthesis gas stream, realizing its maximum utilization.[32]

The above-mentioned studies demonstrate waste polyester fiber being a good alternative to produce activated carbons. In this work, we investigated the influences of nitrogen doping on the structures and surface properties of activated carbon using waste polyester fabrics as precursors. Four nitrogen-containing sources, including melamine, pyridine, dimethylamine, and pyrrole, were selected, considering their differences in the electronic structures of the nitrogen element. Their physical and chemical properties are shown in Table S1.† The content and chemical valence states of the doped nitrogen atoms were compared, and their effects on the adsorption properties towards typical VOCs in the gas phase under both dry and wet conditions were studied. Benzene and ethyl acetate were selected as representatives of nonpolar and polar VOCs because of their wide application in the spraying and coating industries.[33,34] The results would be helpful in providing deeper insights in the preparation of nitrogen-doping carbons from waste fabrics and are beneficial to understanding the adsorption mechanism of nitrogen-containing functional groups.

## 2. Materials and methods

### 2.1 Chemicals and raw fabric

Polyester textile was bought from Ourui Textile Technology Co., Ltd (Hebei, China) and was thoroughly washed with distilled water before use. Zinc chloride, hydrochloric acid (38.0%), pyridine, aqueous dimethylamine solution (40%), melamine and pyrrole were purchased from Macklin Biochemical Technology Company (Shanghai, China). All the reagents are AR grade and were used as received.

### 2.2 Carbon preparation

The preparation of porous carbon included the carbonization and activation processes. Generally, a certain quantity of polyester fabrics was transferred into a tube furnace and was carbonized at 900 °C under a nitrogen atmosphere for 2 h with the flow rate being 50 mL min$^{-1}$. The carbonized sample (5 g) was ground into powder, then 1.5 g of zinc chloride and 5 mL of deionized water were added. The mixture was oscillated ultrasonically for 15 minutes so that the zinc chloride sufficiently entered the micropores. Subsequently, the suspended mixture was dried in the tube furnace at 100 °C for 30 min and then activated at 900 °C for 2 h. The carbons were washed with 10% HCl solution and deionized water repeatedly to completely remove the residual ZnCl$_2$ until the water was neutral. Finally, activated carbons were obtained after drying at 100 °C for 2 h.

### 2.3 Nitrogen doping in carbons

Specifically, 5 g of the activated carbon was immersed in 5 mL of deionized water, then a certain amount of nitrogen source was added. After going through the same heating procedure, the nitrogen-doped carbon was obtained. The molar numbers of nitrogen in various nitrogen sources were calculated to be about 5 times the oxygen content in the activated carbon, and the final synthesized carbons were abbreviated as C-M, C-P, C-D, and C-Y, where the letters M, P, D, and Y refer to melamine, pyridine, dimethylamine, and pyrrole, respectively.

## 2.4 Characterization of carbons

The textural properties of the carbons were measured on an ASAP 2460 aperture analyzer (Micromeritics, USA). Before analyzing, the carbons were degassed under 200 °C for 3 h to remove physically adsorbed water and other gaseous impurities. The specific surface area ($S_{BET}$) was measured using the Brunauer–Emmet–Teller (BET) equation in a relative pressure ($P/P_0$) range of 0.05–0.35. The total pore volume ($V_t$) was estimated at a relative pressure of 0.99 on the nitrogen adsorption/desorption isotherms. The microporous volume ($V_{mic}$) was calculated through the t-plot method, and subtracting micropore volume from the total pore volume equaled the mesoporous volume. The pore size distributions of the carbons were derived based on the non-local density functional theory (NLDFT) using the $N_2$ adsorption isotherm.[19]

The elemental compositions and the valence distribution on the carbons were recorded using an X-ray photoelectron spectrometer (XPS) system (Thermo Fisher, USA). The excitation energy of the monochromatic Al-Kα (12 kV, 6 mA) source is 1486.6 eV and the spot size is 400 μm. For the survey spectra, a pass energy of 150 eV and a step size of 1 eV were used. High-resolution (HR) spectra were recorded by setting the pass energy to be 50 eV at a step size of 0.1 eV. All the peaks were calibrated with respect to the C 1s peak at 284.8 eV. After analyzing, the experimental data were processed using XPSPEAK software. The thermal stability of the carbons was measured by a thermogravimetry analyzer (TG/DTA6300, Hitachi, Japan). The samples were heated from 25 °C to 800 °C in air flow with a ramping rate of 5 °C min$^{-1}$, and the flow rate of the carrier gas was 30 mL min$^{-1}$.

## 2.5 Dynamic adsorption of VOCs

The adsorption properties of carbons were evaluated through a self-assembled dynamic adsorption device, as shown in Fig. 1. Specifically, standard gas containing a certain concentration of benzene or ethyl acetate was mixed with nitrogen to accurately adjust its concentration. The mixed gas passed through a mass flow controller (MFC) and then continued through a U-shaped tube. 50 mg of the carbons with diameters about 0.25 to

0.45 mm were placed in the tube to make a simple adsorption bed, which was then dried in a vacuum oven at 150 °C for 3 hours to remove the residual moisture and other small gaseous molecules. During each adsorption process, the flow rate of the mixed gas was set to 50 mL min$^{-1}$, and the temperature was kept at 25 °C. The inlet concentration ($C_i$) of VOCs was 300 ppmv, and the outlet concentration ($C_o$) after adsorption was analyzed by a gas chromatograph every 5 minutes until the outlet concentration of VOCs reached 95% of the inlet. In the competitive adsorption process, the concentrations of benzene and ethyl acetate were both 150 ppmv. The adsorbed amounts of VOCs onto various carbons can be calculated through the following equation[35]

$$Q = \frac{F}{Mw}\left(C_i t_s - \int_0^{t_s} C_o \mathrm{d}t\right), \tag{1}$$

where $Q$ is the adsorbed amount in mg g$^{-1}$, $F$ is the flowrate of VOCs gases in mL min$^{-1}$, $M$ is the relative molecular mass of the adsorbate, $w$ is the net weight of the adsorbent in g, $C_i$ is the initial concentration of VOCs while $C_o$ is the outlet concentration of VOCs after adsorption in ppmv, and $t_s$ is the saturation time of the adsorption process in min.

## 3. Results and discussion

### 3.1 Materials characteristic

The nitrogen adsorption and desorption isotherms of the carbons are shown in Fig. 2a. According to the classification of IUPAC,[36] all the isotherms display mixed characteristics of type I and type IV, suggesting the coexistence of micropores and mesopores. At the lower relative pressure stage ($P/P_0 < 0.1$), the adsorbed nitrogen quantities increase rapidly, and this is assigned to the micropore filling effect.[37] The different quantities indicate the change in micropore volumes after the activation process. Compared with the original carbon, the addition of nitrogen sources reduced the surface areas and pore volumes, except that dimethylamine realized an expansion. Table 1 lists the textural properties of the pristine and nitrogen-doped carbons. The corresponding specific surface areas of C-M, C-P, C-D, and C-Y were about 32.6%, 72.2%, 142% and 14.3% that of the original carbon of 188.7 cm$^2$ g$^{-1}$. The slight increase at the high relative pressure stage ($P/P_0 > 0.9$) in each isotherm demonstrates there are also a few macropores generated. The pore size distribution curves of the carbons, shown in Fig. 2b, are mainly concentrated at 0.6–2 nm and 10–80 nm. In the range of 0.6–2 nm, the vertical coordinates of all curves are lower than those of the original carbon, manifesting the decrease in micropore volumes, and this is consistent with the parameters listed in Table 1. Pérez-Ramírez et al. proposed the concept of hierarchy factor (HF), which was determined as ($V_{mic}/V_t$) × ($S_{mes}/S_{BET}$), to evaluate the variation of micropores and mesopores in nanomaterials.[38] The HF values of all the carbons are also shown in Table 1. Generally, all the values are smaller than 0.1, indicating all the carbons are mainly microporous. Carbons modified with melamine, pyridine, and pyrrole have HF values close to that of the original carbon, suggesting their micropore volumes and mesopore volumes might
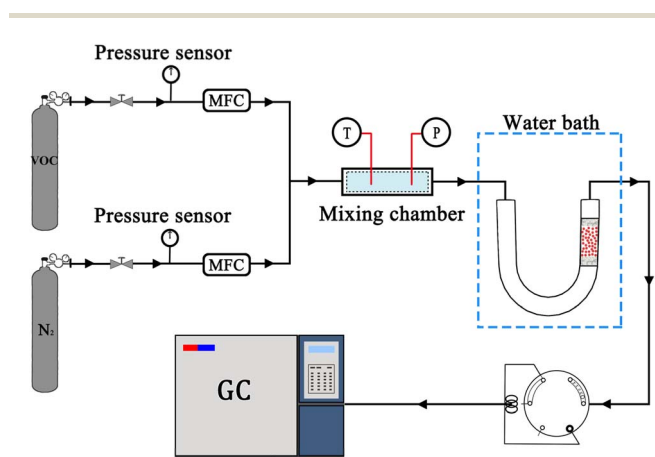


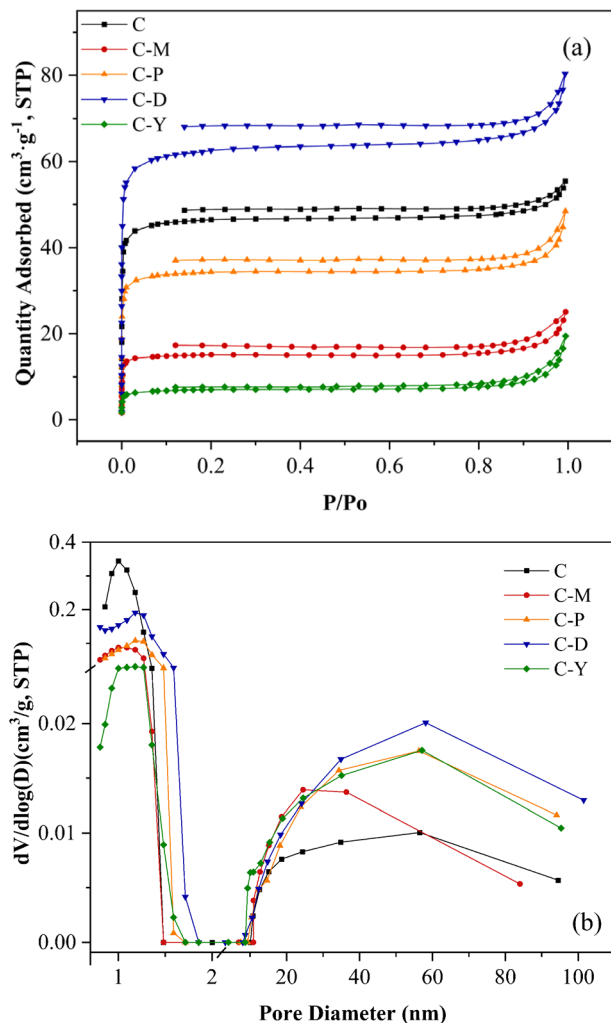Fig. 1 A schematic of the dynamic adsorption device.

**RSC Advances**

**Paper**

Fig. 2 (a) The nitrogen adsorption–desorption isotherms (b) and the pore size distribution curves of the pristine and nitrogen-doped carbons.

decrease in equal proportion. In contrast, dimethylamine promoted the modified carbon to produce a higher HF value, indicating a higher growth rate of mesopores than micropores.[39]

The TG and DTG curves of the activated carbon before nitrogen doping are shown in Fig. S1.† According to the change of the sample weight, obvious weight loss mainly occurred in the temperature range of 450 to 670 °C. The DTG curve represents the relationship between the carbon quantity change rate

and the temperature, and the peak of the curve shows that the rate of weight loss reached the highest near 575 °C. The single peak indicates that the material is mainly composed of carbon with almost no impurities.

XPS was used to analyze the relative contents and chemical valence states of elements. The XPS spectra of the pristine and the nitrogen-modified carbon are shown in Fig. 3, and the calculated contents of nitrogen are listed in Table 2. Clearly, the fewer number of peaks in Fig. 3a reflects that carbon and oxygen are the main elements in the pristine activated carbon. After adding melamine in the activation procedure, nitrogen atoms were successfully introduced into the carbon and the peak intensity of nitrogen had an obvious increase. However, despite all the nitrogen sources added having the same molar number relative to the pristine carbon, the final residual nitrogen contents are quite different from each other. The amount of nitrogen in melamine-modified carbon increased the most, indicating that melamine was a good nitrogen source for preparing nitrogen-doped carbon.[40] The nitrogen content of C-Y was about 2 times that of the pristine carbon, while for pyridine and dimethylamine, fewer nitrogen atoms were introduced. A further deconvolution was performed to distinguish the contents of nitrogen with various chemical valence states. For example, the N 1s spectra of C-M had peaks at about 402.3 eV, 399.6 eV, and 397.9 eV, which can be assigned to oxidized nitrogen, pyrrolic nitrogen, and pyridinic nitrogen, respectively.[33,41] The other doped carbons also contain nitrogen with different chemical valences, of which pyrrolic nitrogen and pyridinic nitrogen are the main species, as shown in Table 2.

### 3.2 Single component adsorption

The dynamic breakthrough curves of benzene and ethyl acetate on the carbons under relative humidities of 0% and 70% are shown in Fig. 4, and they were fitted by the Yoon–Nelson (Y–N) model equation. The Y–N model is widely used to analyze and predict the whole adsorption process, because of its obvious advantages such as simpler digital expression and no need for detailed parameters of fixed bed and adsorbate. It can be described by the following equation,[42]

$$\frac{C_o}{C_i} = \frac{1}{1 + \exp[K(\tau_0 - t)]} \quad (2)$$

where $C_i$ and $C_o$ are the VOCs concentrations at the inlet and outlet of the adsorption bed in ppmv, $K$ is the rate constant reflecting the diffusion characteristics of the mass transfer zone in $\min^{-1}$, and $\tau_0$ is the time required to reach 50% of the inlet concentration in min. Table 3 lists the Y–N parameters of

**Table 1** Textural properties of the pristine and the nitrogen-doped carbons

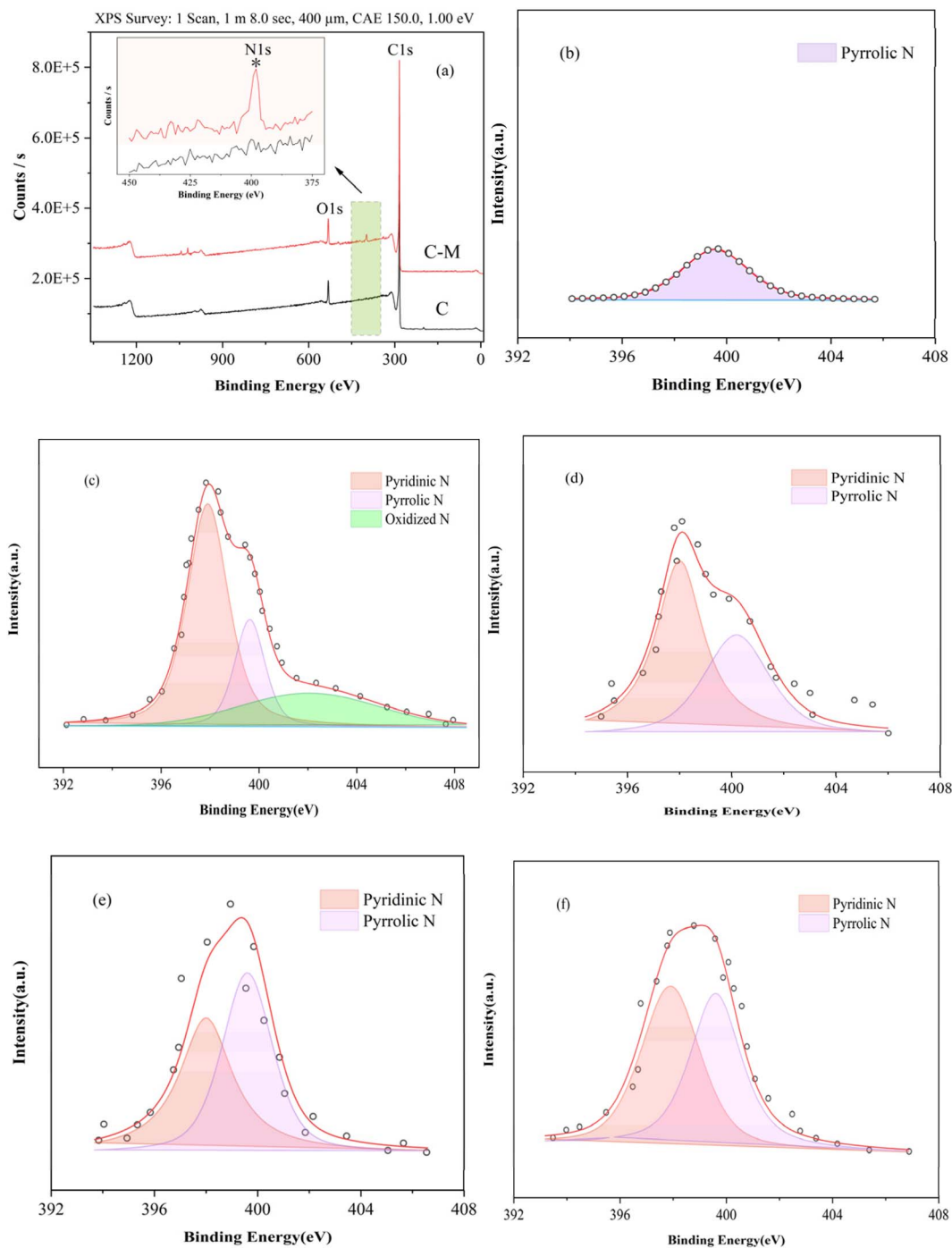| Sample | $S_{BET}$ (m$^2$ g$^{-1}$) | $S_{mic}$ (m$^2$ g$^{-1}$) | $S_{mes}$ (m$^2$ g$^{-1}$) | $V_t$ (cm$^3$ g$^{-1}$) | $V_{mic}$ (cm$^3$ g$^{-1}$) | $V_{mes}$ (cm$^3$ g$^{-1}$) | HF |
|---|---|---|---|---|---|---|---|
| C | 188.7 | 176.1 | 12.6 | 0.09 | 0.07 | 0.02 | 0.05 |
| C-M | 61.6 | 56.1 | 5.5 | 0.04 | 0.02 | 0.02 | 0.04 |
| C-P | 136.2 | 125.8 | 10.4 | 0.07 | 0.05 | 0.02 | 0.05 |
| C-D | 246.8 | 214.1 | 32.7 | 0.12 | 0.08 | 0.04 | 0.09 |
| C-Y | 26.9 | 23.3 | 3.6 | 0.03 | 0.01 | 0.02 | 0.04 |

Fig. 3  (a) XPS spectra of the pristine carbon and C-M; the N 1s XPS spectra of (b) C, (c) C-M, (d) C-P, (e) C-D, and (f) C-Y.

Table 2  Surface element composition of the pristine and nitrogen-doped carbons

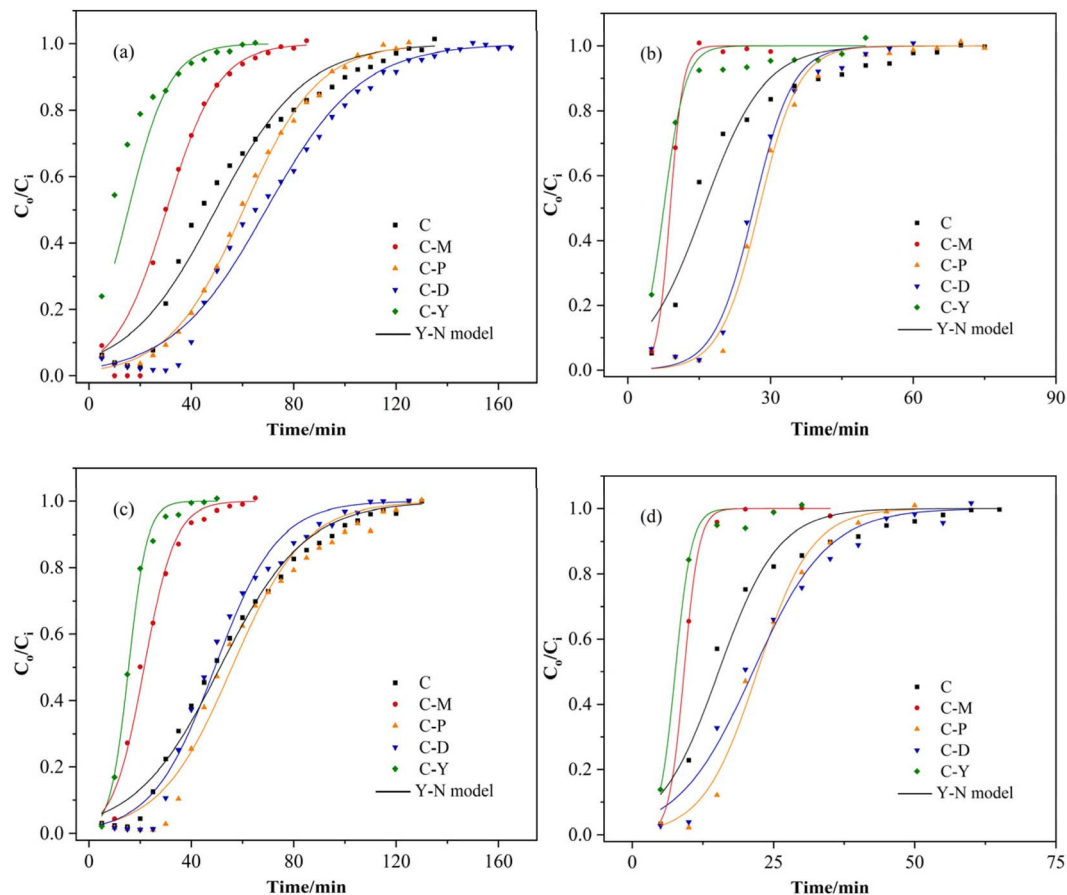| Sample | C/at% | O/at% | N/at% | Pyrrolic N/at% | Pyridinic N/at% | Oxidized N/at% |
|---|---|---|---|---|---|---|
| C | 92.93 | 6.14 | 0.93 | 0.93 | 0 | 0 |
| C-M | 90.58 | 6.26 | 3.17 | 0.61 | 1.81 | 0.75 |
| C-P | 91.76 | 7.14 | 1.09 | 0.43 | 0.66 | 0 |
| C-D | 92.87 | 6.06 | 1.07 | 0.54 | 0.53 | 0 |
| C-Y | 91.7 | 6.14 | 2.16 | 1.04 | 1.12 | 0 |

Fig. 4  Dynamic breakthrough curves of carbons for (a) benzene with RH0%, (b) benzene with RH70%, (c) ethyl acetate with RH0%, and (d) ethyl acetate with RH70%.

benzene and ethyl acetate on all the carbons under different relative humidities at 25 °C. Most of the correlation coefficients are around 0.98, indicating that the Y–N model fitted well to describe the adsorption process. For benzene adsorption, the $\tau_0$ values of C-P and C-D are longer than those of the pristine carbon, while C-M and C-Y show shorter times. Generally, a longer $\tau_0$ value represents a larger adsorbed amount;[42] thus, the adsorbed amounts of benzene follow the order of C-D > C-P

> C > C-M > C-Y. Additionally, the $K$ values of C-P and C-D are approximate to that of the pristine carbon, indicating that their adsorption rates are not decreased. Therefore, a conclusion can be drawn that the adsorption of benzene on carbons modified by dimethylamine and pyridine is faster and larger than that on unmodified carbon. In contrast, when the relative humidity increased to 70%, the rate constant $K$ of all the carbons increased by 2–4 times, showing that the adsorption process

**Table 3**  Y–N parameters of benzene and ethyl acetate on carbons at 298 K

| Sample | Relative humidity (%) | Benzene | | | Ethyl acetate | | |
|---|---|---|---|---|---|---|---|
| | | $K$ (min$^{-1}$) | $\tau_0$ (min) | $R^2$ | $K$ (min$^{-1}$) | $\tau_0$ (min) | $R^2$ |
| C | 0 | 0.058 | 49.57 | 0.971 | 0.060 | 51.25 | 0.988 |
| | 70 | 0.158 | 15.95 | 0.944 | 0.191 | 15.28 | 0.962 |
| C-M | 0 | 0.099 | 30.38 | 0.998 | 0.164 | 21.58 | 0.989 |
| | 70 | 0.733 | 8.92 | 0.998 | 0.754 | 9.17 | 0.998 |
| C-P | 0 | 0.069 | 60.35 | 0.998 | 0.070 | 55.86 | 0.979 |
| | 70 | 0.242 | 27.61 | 0.992 | 0.208 | 22.11 | 0.989 |
| C-D | 0 | 0.054 | 69.20 | 0.988 | 0.081 | 49.23 | 0.984 |
| | 70 | 0.242 | 26.43 | 0.991 | 0.152 | 21.35 | 0.980 |
| C-Y | 0 | 0.124 | 15.41 | 0.956 | 0.275 | 15.50 | 0.995 |
| | 70 | 0.440 | 7.57 | 0.962 | 0.693 | 7.61 | 0.990 |

reaches saturation quickly under a wet atmosphere. The adsorption of ethyl acetate on all the carbons displays the same trend as benzene under both dry and wet atmospheres. These results are consistent with previous studies that water molecules have a detrimental effect on the adsorption of VOCs by activated carbons, especially under high relative humidity conditions.[22,43]

For the sake of comparison, the adsorbed amounts of benzene and ethyl acetate under dry and wet conditions and their ratios are listed in Table 4. Obviously, the adsorbed amounts of the two adsorbates on C-P and C-D are larger than the others. Compared with pristine carbon, the adsorbed amount of benzene on C-P and C-D increased from 50.98 mg g$^{-1}$ to 58.30 mg g$^{-1}$ and 68.20 mg g$^{-1}$, respectively. However, the adsorbed amount of ethyl acetate on C-P and C-D remained almost unchanged, suggesting that the doped nitrogen functional groups have a higher promoting effect on benzene adsorption than ethyl acetate. The ratios of adsorption capacities under wet conditions to those under dry reflect their water resistance. As seen in Table 4, the adsorbed amounts of benzene and ethyl acetate on the pristine carbon decreased more than those of C-D and C-Y under the condition of high humidity. Thus, it can be concluded that the water-resistant abilities of carbons after nitrogen doping improved to a certain extent, especially when pyridine, dimethylamine and pyrrole were used as nitrogen sources. This may be attributed to the doping of nitrogen increasing the hydrophobicity of carbon.[20,21] However, it is worth noting that the water resistance of C-M towards benzene decreased from 36.0% to 26.6% when the relative humidity increased to 70%, which was quite different from other carbons. Similar phenomena have also been reported when using melamine as a nitrogen source to prepare nitrogen-doped carbon.[22,44] The specific reason is still unclear and requires further research. One possible mechanism lies in pyridinic and pyrrolic nitrogen promoting the electrostatic interactions between the activated carbons and water molecules and thus suppressing the adsorption of benzene molecules.[44]

The relationship between the adsorbed amounts of benzene and their structural parameters as well as the compositions are shown in Fig. 5 to reveal the main factors affecting the adsorption performances of the activated carbons. Generally, the adsorbed amounts of benzene on various carbons represent a linear and positive correlation with the structural parameters, including the specific surface area, total pore volume,

micropore surface area, and micropore volume. The adjusted correlation coefficients are in the range of 0.799 to 0.824, implying that the physical properties of carbons mainly determine their adsorbed amounts towards benzene.[45,46] However, no obvious correlation exists between the adsorbed amount of benzene and the surface nitrogen and oxygen contents, considering their correlation coefficients are only 0.409 and −0.246, respectively. The influences of structural parameters and the nitrogen and oxygen contents on the adsorbed amounts of carbons towards ethyl acetate show a similar trend (Fig. S3†), with the biggest difference being exhibiting lower correlation coefficients, which are mainly in the range of 0.533 to 0.697. This suggests that the pore structure is the most important factor affecting the adsorption capacity towards ethyl acetate, yet the influence is smaller than that on benzene.

Previous studies have shown that the porous structure and element composition are the main factors affecting the adsorption performance of activated carbons,[11,12] but the influence of nitrogen content in this work was not significant. In order to clarify the individual contribution of nitrogen functional groups on the adsorption performances of benzene and ethyl acetate, the adsorption capacities of carbons are normalized to the specific surface area,[25] and Pearson correlation analysis is conducted. Pearson correlation analysis is capable of calculating the Pearson correlation coefficients (PCC), which quantitatively assess the linear correlation between any two variables and can be described as[47]

$$r = \frac{\sum_{i=1}^{n}(x_i - \bar{x})\sum_{i=1}^{n}(y_i - \bar{y})}{\sqrt{\sum_{i=1}^{n}(x_i - \bar{x})^2}\sqrt{\sum_{i=1}^{n}(y_i - \bar{y})^2}} \quad (3)$$

where $r$ is the PCC value in the range of −1 to 1. When the correlation coefficient is greater than 0, the two variables are positively correlated. Otherwise, the two variables are negatively correlated. The closer the PCC value is to −1 or 1, the stronger the correlation is.[48]

Fig. 6 shows the Pearson correlation matrices between any two of the influencing factors, including the adsorbed amount per unit surface area and the element composition. The red and blue colors in the correlation matrix diagram represent positive and negative correlations, respectively, and the numbers on the circle represent the degree of correlation. For benzene

**Table 4** Adsorbed amount of benzene and ethyl acetate on carbons under dry ($Q_{RH} = 0\%$) and wet ($Q_{RH} = 70\%$) conditions

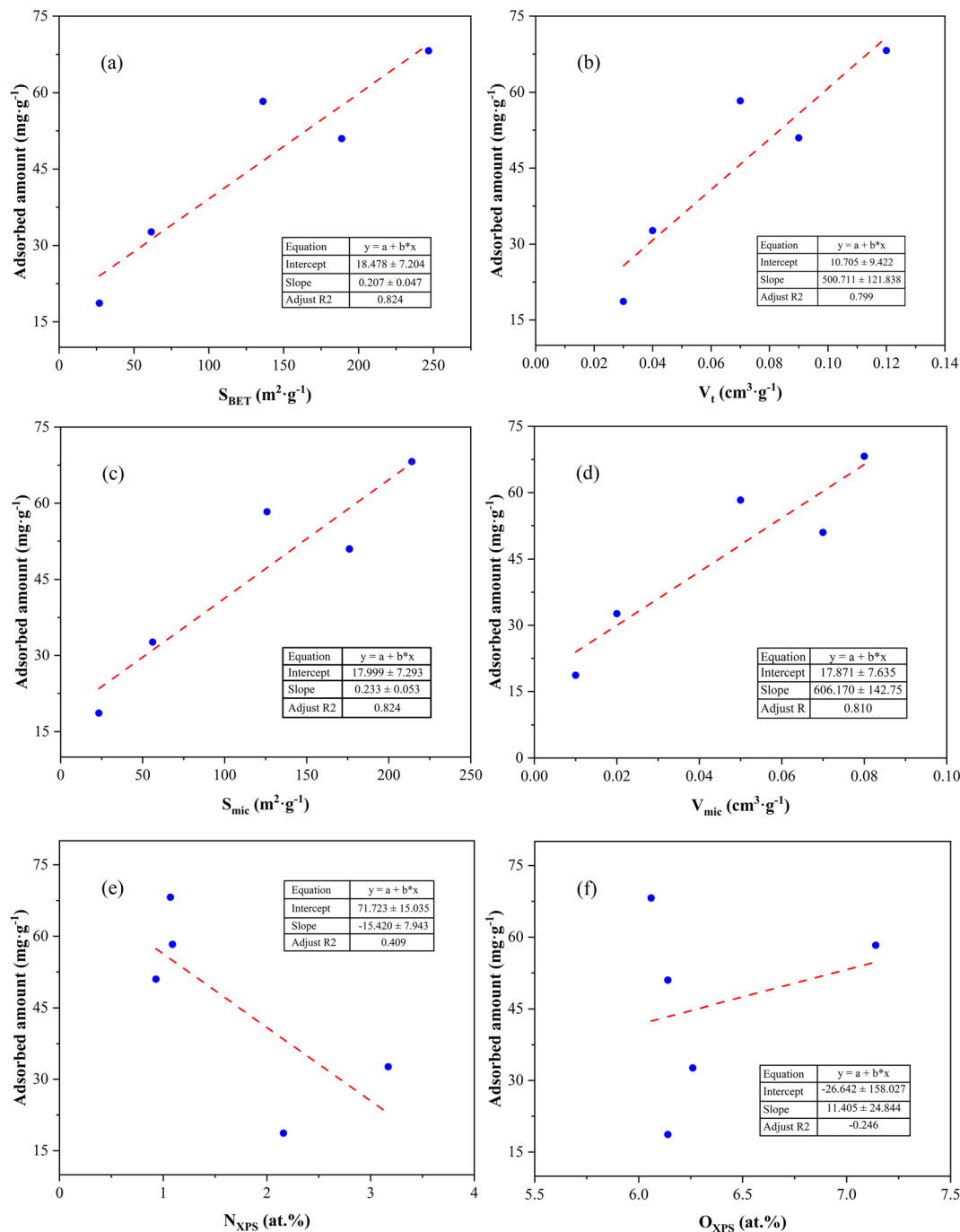| Adsorbed amount (mg g$^{-1}$) | Benzene | | | Ethyl acetate | | |
|---|---|---|---|---|---|---|
| | $Q_{RH} = 0\%$ | $Q_{RH} = 70\%$ | $Q_{wet}/Q_{dry}$ (%) | $Q_{RH} = 0\%$ | $Q_{RH} = 70\%$ | $Q_{wet}/Q_{dry}$ (%) |
| C | 50.98 | 18.32 | 36.0 | 57.98 | 19.21 | 33.1 |
| C-M | 32.64 | 8.68 | 26.6 | 24.60 | 10.23 | 41.6 |
| C-P | 58.30 | 27.01 | 46.3 | 63.68 | 24.67 | 38.8 |
| C-D | 68.20 | 25.94 | 38.0 | 55.88 | 24.55 | 43.9 |
| C-Y | 18.67 | 9.49 | 50.8 | 17.59 | 9.21 | 52.4 |

Fig. 5 Relationship between the adsorbed amount of benzene and (a) the BET specific surface area, (b) pore volume, (c) micropore specific surface area, (d) micropore volume, (e) nitrogen content, (f) oxygen content.

adsorption under dry condition, the correlation coefficients of the nitrogen content and the pyridinic nitrogen were about 0.7, indicating a strong positive correlation. In contrast, the coefficient of pyrrolic nitrogen is 0.36, suggesting that pyridinic nitrogen is more beneficial to benzene adsorption than pyrrolic nitrogen. This result is consistent with previous studies and may be attributed to the stronger π–π interaction and N–H hydrogen bond, which are greater than those of pyrrolic nitrogen.[19,49] However, the water resistance of the pyridinic nitrogen was inferior. When the relative humidity increased to 70%, the correlation coefficient of pyrrolic nitrogen remained basically unchanged, while that of pyridinic nitrogen decreased greatly from 0.73 to 0.35. In the case of ethyl acetate, the influence of nitrogen is quite different. The pyridinic and pyrrolic nitrogen represent weak positive correlation under both dry and wet conditions, and the π–π interaction for the enhancement of ethyl acetate adsorption is not as obvious as that of benzene. This is reasonable considering the polar nature
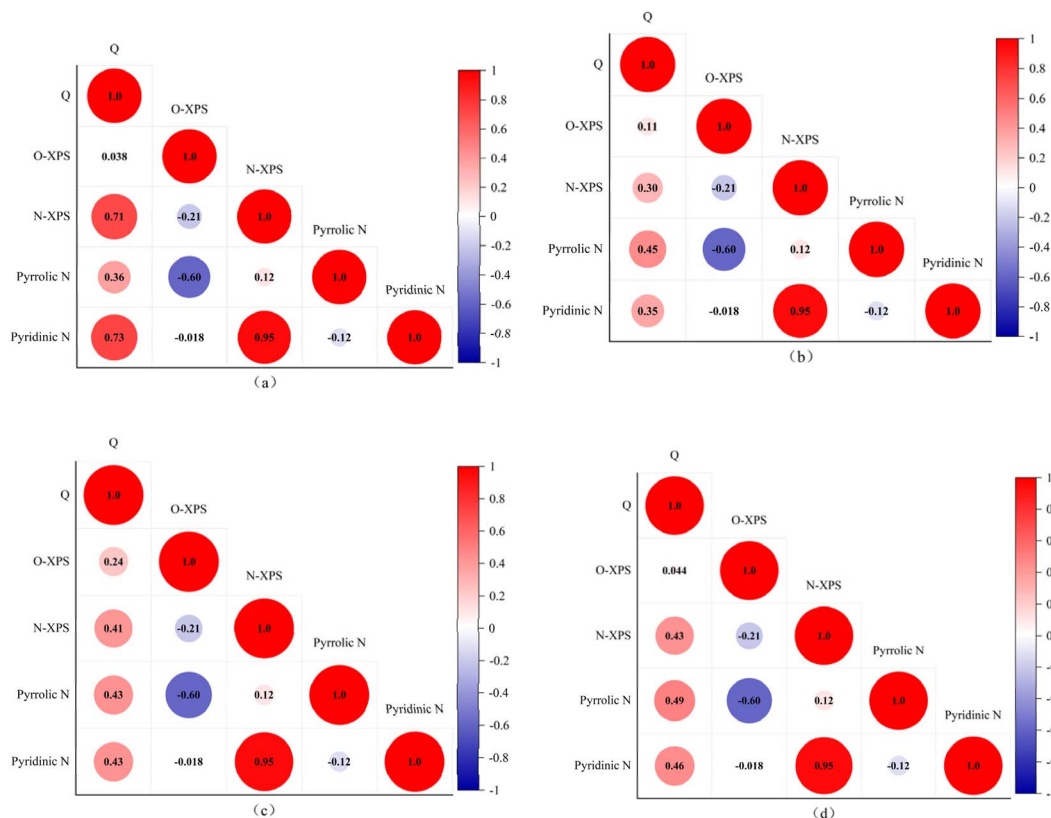
**Fig. 6** Pearson correlation matrices of the adsorbed amount and the element composition: (a) benzene, RH0%; (b) benzene, RH70%; (c) ethyl acetate, RH0%; (d) ethyl acetate, RH70%.

of ethyl acetate. Additionally, the unchanged coefficients implied that nitrogen may not be involved in the formation of hydrogen bonds under the high humidity atmosphere.

### 3.3 Binary-component adsorption of VOCs

Fig. 7 shows the binary-component breakthrough curves and the corresponding Y–N models on all the carbons. Generally, the overall change trends of all the curves were consistent with those of the single component, as shown in Fig. 4. C-D and C-P



**Fig. 7** Breakthrough curves of benzene and ethyl acetate on all the carbons.

adsorbed more benzene and ethyl acetate than the unmodified carbon, while C-M and C-Y reduced the adsorbed amounts. The calculated dynamic adsorbed amounts in the binary system are shown in Table 5, where $Q_B$ and $Q_E$ are the adsorbed amounts of benzene and ethyl acetate, respectively. All the carbons adsorbed a little more ethyl acetate than benzene. The $Q_B/Q_E$ values of C-P and C-D are about 0.85, which are slightly higher than the pristine carbon, further verifying the promotion effect of the pyridinic nitrogen towards benzene adsorption, as they increased after the nitrogen-doping process.
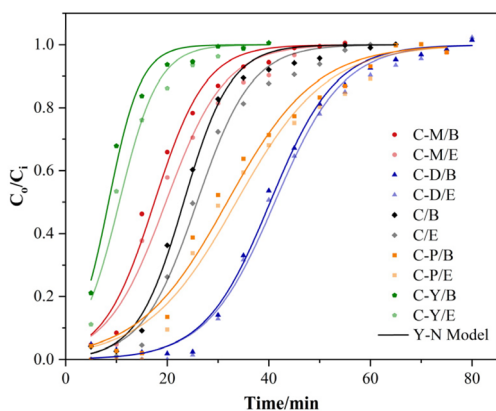
### 3.4 Regeneration ability

The adsorption capacity of each sample for benzene was repeatedly tested five times to investigate the regeneration and re-use properties of all the carbons. After each adsorption, the saturated carbons were heated at 150 °C under vacuum for 3 hours to fully degas the adsorbed benzene molecules. The recycling efficiencies, defined as the ratio of the recycled amount to the amount adsorbed the first time, are shown in Fig. 8. With the increase in the number of cycles, the adsorption capacities of all the samples decreased due to the pore blocking caused by irreversible adsorption. After five consecutive adsorption cycles, the adsorption capacities of all the carbons remained at about 70–75%, except that C-D decreased to only about 55%. Considering that the adsorption capacities increased significantly after modification by pyridine and

**Table 5** Adsorbed amounts and Y–N parameters of benzene and ethyl acetate in binary-component systems

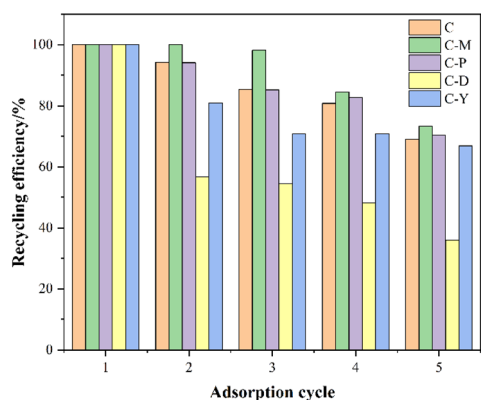| Sample | Benzene | | | | Ethyl acetate | | | | |
|---|---|---|---|---|---|---|---|---|---|
| | $K$ (min$^{-1}$) | $\tau$ (min) | $Q_B$ | $R^2$ | $K$ (min$^{-1}$) | $\tau$ (min) | $Q_E$ | $R^2$ | $Q_B/Q_E$ |
| C | 0.217 | 23.24 | 11.66 | 0.993 | 0.186 | 25.87 | 14.72 | 0.989 | 0.79 |
| C-M | 0.198 | 17.48 | 9.00 | 0.979 | 0.172 | 19.73 | 11.43 | 0.973 | 0.79 |
| C-P | 0.114 | 31.80 | 15.91 | 0.978 | 0.113 | 33.58 | 18.99 | 0.974 | 0.84 |
| C-D | 0.154 | 40.26 | 21.99 | 0.995 | 0.148 | 41.17 | 25.61 | 0.993 | 0.86 |
| C-Y | 0.315 | 8.46 | 4.82 | 0.977 | 0.260 | 10.57 | 6.47 | 0.974 | 0.75 |



**Fig. 8** Removal rate of benzene on carbons for five consecutive cycles under dry conditions.

dimethylamine (as shown in Table 4), it can be concluded that C-P has better adsorption performance after a comprehensive comparison.

# 4. Conclusions

Using polyester fabrics as precursors, activated carbon can be prepared through carbonization and activation. During the activation process, melamine, pyridine, dimethylamine, and pyrrole were selected as nitrogen sources, and nitrogen atoms were successfully doped into the carbons. The nitrogen contents of carbons after doping by melamine (C-M), pyridine (C-P), dimethylamine (C-D), and pyrrole (C-Y) were about 3.4 times, 2.3 times, 1.2 times, and 1.2 times that of the original carbon, and their corresponding specific surface areas were about 32.6%, 72.2%, 142% and 14.3%, respectively, that of the original carbon of 188.7 cm$^2$ g$^{-1}$. The adsorbed amounts of benzene on carbons increased more than those of ethyl acetate under dry condition, suggesting that the promotion effect of nitrogen functional groups on benzene is higher than on ethyl acetate. Correlation analysis between the adsorbed amounts and structural parameters revealed that specific surface area and pore volume mainly determine the adsorption capacities of carbons. Pearson correlation analysis on the normalized adsorbed amount of benzene per surface area verified that the contribution of pyridinic nitrogen was more significant than that of pyrrolic nitrogen, yet the resistance of pyridinic nitrogen to humidity was inferior. Carbon modified by pyridine has the best recycling performance, and, after five adsorption cycles,

the adsorption capacity of benzene carbon remained about 75% of the original. These comprehensive analyses identify pyridine as a good candidate for the nitrogen modification of activated carbon in practical applications.

# Data availability

Data will be made available on request.

# Author contribution

Gang Wang: writing – review & editing, validation, methodology. Ziyan Kong: visualization, methodology, data curation. Pingping Tan: methodology, writing – original draft, data curation. Jianfang Ao: methodology, data curation. Ran Wang: resources, funding acquisition, writing – review & editing. Zhongshen Zhang: resources, formal analysis. Zhengping Hao: funding acquisition, writing – review & editing.

# Conflicts of interest

The authors declare that they have no known competing financial interests or personal relationships that could have appeared to influence the work reported in this paper.

# Acknowledgements

# References

1 C. He, J. Cheng, X. Zhang, M. Douthwaite, S. Pattisson and Z. Hao, *Chem. Rev.*, 2019, **119**, 4471–4568.
2 Y. Son, *Chem. Eng. J.*, 2017, **316**, 609–622.
3 S. Xiang, J. Liu, W. Tao, K. Yi, J. Xu, X. Hu, H. Liu, Y. Wang, Y. Zhang, H. Yang, J. Hu, Y. Wan, X. Wang, J. Ma, X. Wang and S. Tao, *Atmos. Environ.*, 2020, **224**, 117259.
4 L. Kong, M. Song, X. Li, Y. Liu, S. Lu, L. Zeng and Y. Zhang, *J. Environ. Sci.*, 2024, **138**, 385–394.

5 P. Wang, Y. Chen, J. Hu, H. Zhang and Q. Ying, *Environ. Sci. Technol.*, 2019, **53**, 1404–1412.

6 Q. Zhao, Y. Li, X. Chai, L. Xu, L. Zhang, P. Ning, J. Huang and S. Tian, *J. Hazard. Mater.*, 2019, **369**, 512–520.

7 H. Jang, J. Cho and C. Kim, *Environ. Res.*, 2024, **259**, 119586.

8 H. Wang, S. Sun, L. Nie, Z. Zhang, W. Li and Z. Hao, *J. Environ. Sci.*, 2023, **123**, 127–139.

9 F. Pan, W. Zhang, C. Ferronato, J. Valverde and A. Giroir-Fendler, *Appl. Catal., B*, 2024, **342**, 123406.

10 J. González-Martín, S. Cantera, R. Muñoz and R. Lebrero, *J. Environ. Manage.*, 2024, **349**, 119362.

11 G. Wang, Z. Zhang and Z. Hao, *Crit. Rev. Env. Sci. Tec.*, 2019, **49**, 2257–2313.

12 X. Zhang, B. Gao, A. Creamer, C. Cao and Y. Li, *J. Hazard. Mater.*, 2017, **338**, 102–123.

13 E. Frank, L. Steudle, D. Ingildeev, J. Spörl and M. Buchmeiser, *Angew. Chem., Int. Ed.*, 2014, **53**, 5262–5298.

14 L. Zhu, D. Shen and K. Luo, *J. Hazard. Mater.*, 2020, **389**, 122102.

15 X. Ge, Z. Wu, Z. Wu, Y. Yan, G. Cravotto and B. Ye, *J. Ind. Eng. Chem.*, 2016, **39**, 27–36.

16 S. Park, H. Lee, Y. Lee, S. An, J. Yang and J. Kim, *ACS Appl. Nano Mater.*, 2023, **6**, 19611–19621.

17 R. Shi, K. Liu, B. Liu, H. Chen, X. Xu, Y. Ren, J. Qiu, Z. Zeng and Q. Li, *Colloids Surf., A*, 2022, **632**, 124983.

18 L. Li, S. Liu and J. Liu, *J. Hazard. Mater.*, 2011, **192**, 683–690.

19 S. Zhang, Y. Lin, Q. Li, X. Jiang, Z. Huang, X. Wu, H. Zhao, G. Jing and H. Shen, *Sep. Purif. Technol.*, 2022, **289**, 120784.

20 M. Zhu, K. Zhou, X. Sun, Z. Zhao, Z. Tong and Z. Zhao, *Chem. Eng. J.*, 2017, **317**, 660–672.

21 J. Li, T. Cheng, X. Ma, X. Hou, H. Wu and L. Yang, *Environ. Sci. Pollut. Res.*, 2022, **29**, 85257–85270.

22 T. Fan, H. Zhao, Z. Wang, M. He, J. Jia, Z. Sun, L. Yang, W. Zhou, Z. Hu and X. Zhang, *J. Environ. Chem. Eng.*, 2024, **12**, 113667.

23 Y. Jiao, Z. Wang, H. Zhao, E. Meng, Z. Sun, L. Yang, M. He, J. Jia, K. An, X. Pi, S. Shao and J. Zhou, *Appl. Surf. Sci.*, 2024, **670**, 160686.

24 G. Zhao, Y. Wang, L. Xie, S. Wang, Y. Ji, X. Sun, Z. Zhong, W. Peng, H. Huang and D. Ye, *Sep. Purif. Technol.*, 2025, **353**, 128478.

25 B. Liu, L. Yu, H. Wang, X. Ma, Z. Zeng and L. Li, *Chem. Eng. J.*, 2022, **435**, 135069.

26 Y. Rong, C. Pan, K. Song, J. Chol Nam, F. Wu, Z. You, Z. Hao, J. Li and Z. Zhang, *Chem. Eng. J.*, 2023, **461**, 141979.

27 D. Tian, Z. Xu, D. Zhang, Y. Zhou and Z. Sun, *Colloids Surf., A*, 2020, **598**, 124756.

28 Z. Yuan, Z. Xu, D. Zhang, W. Chen, T. Zhang, Y. Huang, L. Gu, H. Deng and D. Tian, *Appl. Surf. Sci.*, 2018, **427**, 340–348.

29 Z. Yuan, Z. Xu, D. Zhang, W. Chen, Y. Huang, T. Zhang, D. Tian, H. Deng, Y. Zhou and Z. Sun, *Colloids Surf., A*, 2018, **549**, 86–93.

30 Z. Xu, D. Tian, Z. Sun, D. Zhang, Y. Zhou, W. Chen and H. Deng, *Colloids Surf., A*, 2019, **565**, 180–187.

31 G. Duman, *J. Water Process. Eng.*, 2021, **43**, 102286.

32 A. Serras-Malillos, B. Perez-Martinez, A. Lopez-Urionabarrenechea, E. Acha and B. Caballero, *Sustain. Mater. Technol.*, 2023, **38**, e00773.

33 L. Tan, J. Wang, B. Cai, C. Wang, Z. Ao and S. Wang, *J. Hazard. Mater.*, 2022, **424**, 127348.

34 S. Niknaddaf, J. Atkinson, P. Shariaty, M. Lashaki, Z. Hashisho, J. Phillips, J. Anderson and M. Nichols, *Carbon*, 2016, **96**, 131–138.

35 Z. Li, Y. Liu, X. Yang, Y. Xing, Q. Yang and R. T. Yang, *Adsorption*, 2017, **23**, 361–371.

36 M. Thommes, K. Kaneko, A. Neimark, J. Olivier, F. Rodriguez-Reinoso, J. Rouquerol and K. Sing, *Pure Appl. Chem.*, 2015, **87**, 1051–1069.

37 B. Liu, X. Ma, D. Wei, Y. Yang, Z. Zeng and L. Li, *Carbon*, 2022, **192**, 41–49.

38 J. Pérez-Ramírez, D. Verboekend, A. Bonilla and S. Abelló, *Adv. Funct. Mater.*, 2009, **19**, 3972–3979.

39 A. Shahid, S. Lopez-Orozco, V. Marthala, M. Hartmann and W. Schwieger, *Microporous Mesoporous Mater.*, 2017, **237**, 151–159.

40 D. Hulicova, J. Yamashita, Y. Soneda, H. Hatori and M. Kodama, *Chem. Mater.*, 2005, **17**, 1241–1247.

41 J. Qi, Y. Li, G. Wei, J. Li, X. Sun, J. Shen, W. Han and L. Wang, *Sep. Purif. Technol.*, 2017, **188**, 112–118.

42 J. Wang, G. Wang, W. Wang, Z. Zhang, Z. Liu and Z. Hao, *J. Mater. Chem. A*, 2014, **2**, 14028–14037.

43 Y. Huang, Q. Cheng, Z. Wang, S. Liu, C. Zou, J. Guo and X. Guo, *Chem. Eng. J.*, 2020, **398**, 125557.

44 H. Zhao, Z. Tang, Z. Wang, J. Li, Z. Hu, Q. Wang, Q. Yu, X. Zhang, B. Zhou and E. Meng, *Environ. Pollut.*, 2024, **340**, 122819.

45 R. Shi, K. Liu, B. Liu, H. Chen, X. Xu, Y. Ren, J. Qiu, Z. Zeng and L. Li, *Colloids Surf., A*, 2022, **632**, 127600.

46 Y. Jiang, X. Xu, B. Liu, C. Zhou, H. Wang, J. Qiu, Z. Zeng, Y. Ge and L. Li, *Microporous Mesoporous Mater.*, 2022, **341**, 112081.

47 X. Ma, W. Xu, R. Su, L. Shao, Z. Zeng, L. Li and H. Wang, *Sep. Purif. Technol.*, 2023, **306**, 122521.

48 S. Zhang, A. Ali, J. Su, T. Huang and M. Li, *Water Res.*, 2022, **209**, 117899.

49 Q. Liu, M. Ke, F. Liu, P. Yu, H. Hu and C. Li, *RSC Adv.*, 2017, **7**, 22892–22899.